HHS Public Access

Author manuscript

ACS Biomater Sci Eng. Author manuscript; available in PMC 2021 September 14.

Published in final edited form as:

ACS Biomater Sci Eng. 2020 September 14; 6(9): 4929–4939. doi:10.1021/acsbiomaterials.0c00845.

Keratinocyte-Specific Peptide-Based Surfaces for Hemidesmosome Upregulation and Prevention of Bacterial Colonization

Nicholas G. Fischer,
MDRCBB-Minnesota Dental Research Center for Biomaterials and Biomechanics, University of Minnesota, Minneapolis, Minnesota 55455, United States

Dina G. Moussa,
MDRCBB-Minnesota Dental Research Center for Biomaterials and Biomechanics, University of Minnesota, Minneapolis, Minnesota 55455, United States

Erik P. Skoe,
MDRCBB-Minnesota Dental Research Center for Biomaterials and Biomechanics, University of Minnesota, Minneapolis, Minnesota 55455, United States

David A. De Jong,
MDRCBB-Minnesota Dental Research Center for Biomaterials and Biomechanics, University of Minnesota, Minneapolis, Minnesota 55455, United States

Conrado Aparicio
MDRCBB-Minnesota Dental Research Center for Biomaterials and Biomechanics, University of Minnesota, Minneapolis, Minnesota 55455, United State

Abstract

Percutaneous devices like orthopedic prosthetic implants for amputees, catheters, and dental implants suffer from high infection rates. A critical aspect mediating peri-implant infection of dental implants is the lack of a structural barrier between the soft tissue and the implant surface which could impede bacteria access and colonization of exposed implant surfaces. Parafunctional soft tissue regeneration around dental implants is marked by a lack of hemidesmosome formation

Corresponding Author: Conrado Aparicio – MDRCBB-Minnesota Dental Research Center for Biomaterials and Biomechanics, University of Minnesota, Minneapolis, Minnesota 55455, United States; apari003@umn.edu.

Author Contributions

Nicholas G. Fischer: Conceptualization; Methodology; Validation; Visualization; Writing - Original Draft; Writing - Review and Editing; Investigation. Dina G. Moussa: Methodology; Writing - Review and Editing; Investigation. Erik P. Skoe: Writing - Review and Editing; Investigation. David A. De Jong: Writing - Review and Editing; Investigation. Conrado Aparicio: Conceptualization; Validation; Funding acquisition; Project Administration; Writing - Review and Editing,

The authors declare no competing financial interest.

Data Availability. The raw/processed data required to reproduce these findings will be made available on request.

Complete contact information is available at: https://pubs.acs.org/10.1021/acsbiomaterials.0c00845

Supporting Information

The Supporting Information is available free of charge at https://pubs.acs.org/doi/10.1021/acsbiomaterials.0c00845.

HPLC and mass spectrometry of peptide synthesis, full X-ray photoelectron spectroscopy (XPS) spectra, dynamic surface fractional area for 96L/4G, fluorescent visualization of fluorescently tagged peptides after incubation (37 °C) in saliva through 14 days, experimental schematic of centrifugation experiment, and quantification of elemental composition (atomic %) of coatings and controls (PDF)

and thereby weakened mechanical attachment. In response to this healthcare burden, a simultaneously hemidesmosome-inducing, antimicrobial, multifunctional implant surface was engineered. A designer antimicrobial peptide, GL13K, and a laminin-derived peptide, LamLG3, were coimmobilized with two different surface fractional areas. The coimmobilized peptide surfaces showed antibiofilm activity against *Streptococcus gordonii* while enhancing proliferation, hemidesmosome formation, and mechanical attachment of orally derived keratinocytes. Notably, the coatings demonstrated specific activation of keratinocytes: the coatings showed no effects on gingival fibroblasts which are known to impede the quality of soft tissue attachment to dental implants. These coatings demonstrated stability and retained activity against mechanical and thermochemical challenges, suggesting their intraoral durability. Overall, these multifunctional surfaces may be able to reduce peri-implantitis rates and enhance the success rates of all percutaneous devices via strong antimicrobial activity and enhanced soft tissue attachment to implants.

Graphical Abstract

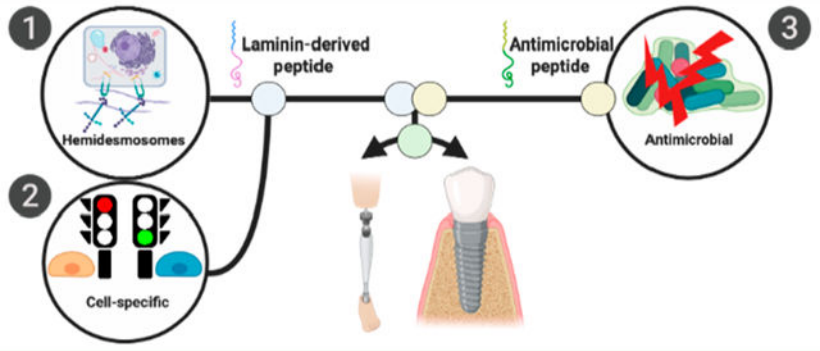

Keywords

peptide; surface; hemidesmosome; keratinocyte; antimicrobial; anti-infection

1. INTRODUCTION

A variety of percutaneous devices, such as catheters, left ventricular assist devices (LVADs), orthopedic prosthetic implants for amputees, and bone anchored hearing aids report infection rates higher than 25%.[1–4] Dental implants, which more than 23% of the entire adult U.S. population may have by 2026,[5] are of particular concern given the ballooning number of implants—over five million are placed in the US each year[6]—and the aging U.S. population.[7–9] Dental implant infection, or peri-implantitis, is an inflammatory process etiologically rooted in biofilm formation affecting supporting tissues around a dental implant.[10,11] Dysbiosis shifts the relative abundance of commensal species toward pathogenicity and results in a marked inflammatory response, dramatic bone loss, and expensive implant removal.[12] Rates of peri-implantitis vary based on different diagnostic thresholds, but a recent meta-analysis reported an implant-based prevalence of 9.25% and a patient-based prevalence of 19.83%.[13] However, treating peri-implantitis is notoriously

difficult.[8] Biomaterial-based innovations are necessary to prevent this pernicious disease and relieve the clinical burden of treating peri-implantitis.[14]

The aforementioned array of infection-prone percutaneous devices experiences the same challenge as dental implants: establishment of a long-lasting structural barrier between the soft tissue and the implant surface to prevent biofilm expansion, infection, and device failure. Nature provides inspiration to address this growing challenge. Teeth, a natural percutaneous organ, have a unique epithelial component, the junctional epithelium (JE), mediating a durable soft tissue attachment to the tooth substratum. Oral keratinocytes (OKs) residing in the JE secrete a basement membrane compositionally unique to that of any other basement membrane in the human body: rich in laminin 332,[15] which serves as an integrin ligand to form hemidesmosomes (HDs) via integrin $\alpha 6\beta 4$ ligation of the $\alpha 3$ chain globular module (LG3) of laminin 332.[16,17] HDs are the transmembrane "links" between teeth and gingiva, while the JE forms a protective barrier for mechanical stability of the tooth, or dental implant, and a physical barrier against biofilm invasion.[18] However, HD formation on dental implants only occurs apically, leaving the implant coronal surface vulnerable to infection.[18] Analogously, striking work shows that when structural JE proteins are knocked out of mice, the resultant "flaky" JE completely detaches from teeth and the onset of periodontitis and infection is remarkably fast.[19] More specifically, individuals with mutations in HD proteins, such as epidermolysis bullosa ("butterfly skin"), display severe periodontal disease.[20] One contributing factor to the parafunctional regeneration of JE on peri-implant surfaces is the colonization of surfaces with fibroblasts and not tissue-native keratinocytes.[21] Similar challenges exist for percutaneous orthopedic implants for which skin attachment is markedly difficult to achieve.[3]

Despite the benefits of enhanced soft tissue attachment on implant surfaces, such a healing process inevitably takes time: typically around 6–8 weeks for dental implants.[22] Thus, dental implants would benefit from a second defense other than enhanced soft tissue healing during early implant healing,[23] a period in which the implant is most vulnerable to biofilm formation. Due to their microbial resistance, an attractive biomolecule to combat biofilm formation is antimicrobial peptides.[24] The self-assembling,[25,26] cationic, amphipathic designer antimicrobial peptides GL13K[27] has demonstrated bactericidal activity against *Porphyromonas gingivalis*, *Escherichia coli*, *Pseudomonas aeruginosa*, *Streptococcus aureus*, *Enterococcus faecalis*, and microcosms, highly cariogenic biofilms, and a primary colonizer of oral and dental implant surfaces, *Streptococcus gordonii*.[25,28–35]

In this work, a peptide (LamLG3) derived[36,37] from the LG3 module of laminin 332 capable of inducing HD formation in OKs and GL13K were coimmobilized on titanium.[38,39] We and others have previously shown that biomolecules retain biological activity when mono- and coimmobilized on titanium[30,38,40,41] using silanization chemistry and rational peptide design.[42] Oligopeptides such as these generally present favorable immunological profiles which may hasten their translation to clinical trials.[43] We hypothesized that surfaces with coimmobilized peptides would be multifunctional by upregulating HDs formation in OKs, displaying antibiofilm potency against *S. gordonii*, and show no effects on gingival fibroblasts (i.e., keratinocyte-specific). Overall, our approach may substantially reduce the

burden of care for a range—from dental implants to orthopedics—of osseointegrated, percutaneous devices.

2. METHODS

2.1. Surface Coatings.

2.1.1. Peptides.—GL13K (GKIIKLKA-SLKLL-NH_2) and LamLG3 (NH_2-KKGGG-PPFLMLLKGSTRFC) were produced (>95% purity; AAPPTec, USA; high-performance liquid chromatography and mass spectrometry characterization in Figure S1 and Figure S2). The N-terminus of LamLG3 was modified with a three glycine spacer plus two lysines to covalently immobilize the peptides with the silanized titanium surfaces. Fluorescently labeled peptides were synthesized by conjugating TAMRA-red and 5,6-FAM-green probe to the C-terminus of LamLG3 and N-terminus of GL13K (>95% purity; AAPPTec, USA), respectively (high-performance liquid chromatography and mass spectrometry characterization in Figures S3 for GL13K-5,6-FAM and Figure S4 for LamLG3-TAMRA).

2.1.2. Titanium Surface Preparation and Immobilization.—Commercially Pure Titanium grade II disks (McMaster-Carr, USA) were punched, ground and polished, activated by etching [5 M NaOH (Sigma-Aldrich, USA), 60 °C, overnight], and cleaned with solvents [deionized water (DI, Milli-Q Plus, USA), isopropanol, and acetone]. These etched disks (eTi) were silanized (eTi-sil) as previously described.[41] Disks were placed under an N_2-rich atmosphere and immersed in 0.05 M *N,N*-diisopropylethylamine and 0.5 M (3-chloropropyl)-triethoxysilane in pentane (all obtained from Sigma-Aldrich, USA) and washed in solvents (ethanol, isopropyl alcohol, DI water, and acetone).

The silanized disks were immersed in 0.1 m M peptide (s) solutions in 0.5 mg/mL Na_2CO_3 overnight and again cleaned with solvents. Co-immobilized disks were obtained at two different surface fractional areas of each peptide: 96% LamLG3/4% GL13K (96L/4G) and 79% LamLG3/21% GL13K. The method for peptide surface fractional area determination is detailed later. The former group was obtained by mixing LamLG3 and GL13K solutions 1:1 (v/v) yielding a pH of 9.42. The latter group was obtained by adjusting the pH of the 1:1 (v/v) solution down to 9.04 to increase the positive charge on GL13K.[25] This favored GL13K peptide recruitment and reaction to the negatively charged eTi-sil sample[42] vs LamLG3.

2.2. Surface Characterization.

2.2.1. Elemental Surface Composition.—A PHI 5000 VersaProbe III (ULVAC Inc., Japan) X-ray photoelectron spectrometer (XPS) was used to measure surface elemental composition with a monochromatic Al Kα X-ray source (45°, 1486.6 eV, 50 W, sampling area; 200 μm diameter). Survey spectra were collected using a pass energy of 280 eV with a step size of 1.0 eV. Charge compensation was used and calibrated with the C 1s signal located at 284.8 eV. Surface elemental composition [as atomic composition (atomic %)] was determined using MultiPak (ULVAC Inc.) from background-subtracted (system optimized) peak areas.

2.2.2. Wettability.—Water contact angles (WCAs) were measured using the sessile-drop (deionized water; 2 μL) method to assess wettability of the surfaces using a contact angle goniometer (DM-CE1, Japan). Dynamic contact angles were also captured at a resolution of 1 s for 15 s, which was experimentally determined to be the end of the dynamic water contact angle response, i.e., quasi-equilibrium using the circle method.

2.2.3. Coimmobilized Peptide Surface Fractional Area.—The fraction of each coimmobilized surface cover by either LamLG3 or GL13K was determined using principles of wetting. Contact angles on macroscopically heterogeneous surfaces are typically estimated using the classic Cassie–Baxter equation.[44,45] However, Israelachvili and Gee[46] proposed an alternative relationship for the water contact angle of surfaces composed of mixed molecules

$$(1+\cos\theta_c)^2 = f_A(1+\cos\theta_A)^2 + f_B(1+\cos\theta_B)^2 \quad (1)$$

where f_A is the projected fractional area occupied by component (i.e., peptide) A and θ_A is the WCA on a homogeneous surface composed of A (likewise for component B) as they, A and B, additively yield θ_C, the WCA of the complete (C) coimmobilized surface.

This model is based on the additivity of molecular polarizabilities, dipoles, and charges and has been validated with atomic force microscopy for immobilized peptides.[47,48] The projected surface fractional area of the surface occupied by each peptide was determined using eq 1 and the previously determined WCAs (Section 2.2.2).

2.2.4. Fluorescently Labeled Peptide Coatings Visualization.—eTi-sil was coated with fluorescently labeled peptides following the previously described protocol (Section 2.1.2) for GL13K, LamLG3, 96L/4G, and 79L/21G. Micrographs were obtained with an upright fluorescent microscope (DM 6B, Leica, Germany) and analyzed in ImageJ (Version 2.0.0-RC-69/1.52K, NIH, USA).

2.2.5. Mechanical and Thermochemical Stability.—All surfaces were mechanically and thermochemically challenged by ultra-sonication in phosphate buffered saline (pH = 7.4 and pH = 4.5; acidic pH to mimic possible biofilm formation) for 1 and 2 h. Surfaces were incubated (37 °C) for 1 week in a similar manner. Finally, surfaces were incubated (37 °C) for 2 weeks in saliva. Unstimulated saliva was collected from the investigator with good oral health (no active caries nor periodontal disease). The saliva was immediately centrifuged twice at 35,280 RCF at 4 °C for 10 min. The supernatant was collected and filtered with 0.22 μm syringe filters, diluted to 25% (v/v) in DI water, and filtered (0.22 μm). Saliva was used immediately after filtration and replaced every 3 days. Samples were washed thrice in PBS between micrograph acquisition.

2.3. Eukaryotic Cell Response.

Immortalized human TERT-2/OKF-6 (OKs; BWH Cell Culture and Microscopy Core, Boston, MA, USA) OKs from non-neoplastic tissue from the floor of the mouth were cultured in defined keratinocyte serum-free media (Gibco, USA) with 1% penicillin/streptomycin (Gibco) under standard conditions.[49] Primary human gingival fibroblasts

(HGFs; PCS-201–018, ATCC, USA) were cultured in low-serum media (ATCC, USA) with 1% penicillin/streptomycin and were used between passages 5 and 7.

2.3.1. OK Immunofluorescence.—OKs were seeded (5×10^4) and cultured for 1 or 3 days and then fixed for 10 min in ice-cold methanol. Cells were immersed in 5% bovine serum albumin (BSA) in PBS and probed with a primary rabbit polyclonal antibody for Collagen XVII [(critical marker for HD assembly[50]) ab28440; Abcam, UK; 1:500] for 1 h at room temperature. After extensive washing, samples were immersed in an anti-rabbit secondary antibody (A11034; Thermo Fisher Scientific, USA; 1:500). Samples were counterstained with DAPI (4′,6-diamidino-2-phenylindole dihydrochloride; D1306; Sigma-Aldrich, USA). Total fluorescent intensity in each field was quantified after subtraction for secondary-only controls at constant settings across all samples. In parallel, samples were stained with rhodamine-conjugated phalloidin (R415; Thermo-Fisher, USA) for 10 min at room temperature and DAPI. Micrographs (×10) were obtained on an upright fluorescent microscope as previously described (Section 2.2.4). Cell surface area was calculated in ImageJ based on Collagen XVII staining.[51] Multiple fields of view (FOVs) were captured per sample.

2.3.2. OK Proliferation.—OKs were seeded as previously described (Section 2.3). Samples were then washed in PBS and incubated for 3 h in CCK8 solution (Dojindo, Japan; 9:1 CCK8:OK media). Optical density (OD; λ = 450 nm) was obtained on a plate reader (Synergy HT, Biotek, USA). OD values were blanked with virgin CCK8 solution similarly incubated to obtain metabolic activity. The number of nuclei were also quantified per FOV to complement metabolic activity (multiple FOVs per sample).

2.3.3. HGF Cell Proliferation.—HGFs (PCS-201–018, ATCC) were seeded (1×10^5) directly onto the samples with 30 μL of cell-laden media. Wells were flooded with media following 30 min in an incubator to allow for cell attachment and then cultured for 2 days. Samples were then prepared for CCK8 metabolic activity measurements as described previously (Section 2.3.2) with a 2 h incubation. The number of nuclei per FOV was also quantified (multiple FOVs for each sample).

2.3.4. OK Mechanical Attachment.—The relative cell adhesion force of OKs on the samples was measured following the work of Reyes and García.[52] OKs were seeded as previously described (Section 2.3). and allowed to proliferate for 2 days. The samples were then placed vertically in custom, 3D-printed holders (Figure S10A; printed with Dental SG Resin, Formlabs, USA) in a wellplate and centrifuged at 500 *g* in culture media. The number of cells was determined by DAPI staining, as previously described (Section 2.3.3), before and after centrifugation on separate samples (multiple FOVs per sample) and expressed as a percentage of cells remaining after centrifugation.

2.4. *S. gordonii* Antibiofilm Activity.

2 mL Bacto Todd-Hewitt broth (BD Biosciences, USA) was inoculated with *S. gordonii* M5 and incubated with 5% CO_2 incubator for 6 h. At the exponential growth phase, OD = 0.7 at λ = 600 nm of the inoculum was measured and then diluted 50-fold with Todd-Hewitt broth.

Samples were disinfected with 70% ethanol (immersed for 3–5 min) followed by an autoclaved Milli-Q water rinse and then left to dry on sterile gauze. Each sample was inoculated with 200 μL of the adjusted inoculum and then 1.8 mL of the fresh media was added. Samples were incubated for 20 h at 37 °C under continuous shaking.

2.4.1. Crystal Violet Biomass.—Samples were washed with 0.9% NaCl solution three times and stained with 0.1% crystal violet for 20 min at room temperature to determine the remaining biomass. Samples were then washed thoroughly with DI water and the remaining dye was eluted into 30% acetic acid. OD values were obtained at λ = 550 nm.

2.4.2. Colony Forming Units.—Colony forming units (CFUs) were determined as an indicator of proliferative bacterial cells. Biofilms were detached from the discs with an ultrasonic scaler (Cavitron Select SPS ultrasonic scaler type Gen-124, Dentsply Sirona, USA) without water irrigation. 1 mL of ice-cold 0.9% NaCl was added to 10 mL glass vials with the samples inside. The openings of the vials were sealed with plastic paraffin film around the ultrasonic insert (Slimline–FSI-SLI 10S, Dentsply Sirona, USA) and then sonicated for 90 s on ice to compensate for the possible heat generation during sonication. The bacterial cells were collected after additional tabletop vortexing. Serial dilutions were prepared (10^1–10^6 in quadruplicate) to be cultured on Bacto Todd-Hewitt granulated agar (BD Biosciences, USA). The plates were incubated at 37 °C for 24 h in the CO_2 chamber and CFU counting was performed.

2.4.3. ATP Bioluminescence Activity.—Adenosine triphosphate (ATP) bioluminescent activity was determined (BacTiter-Glo, Promega, USA) as an indicator of metabolically active bacterial cells. Samples were sonicated for 20 min in 0.9% NaCl (Aristocrat Ultrasonic, USA), and then 100 μL of solution was added to 100 μL of activated reagent. Luminescence (Synergy HT, Biotek, USA) was measured after 5 min of incubation.

2.4.4. LIVE/DEAD.—A LIVE/DEAD assay was performed to visualize cell colonization of surfaces and membrane integrity of all experimental groups. After bacterial culture, samples were washed in 0.9% NaCl and stained on ice in SYTO 9 green stain and propidium iodide red stain in ultrapure water following the manufacturer's instructions (FilmTracer LIVE/DEAD, Thermo-Fisher, USA). Cells with an intact membrane fluoresce green, whereas cells with a compromised membrane, an indication of bacterial death, fluoresce red. Representative images are shown.

2.5. Statistics.

Mean values were compared with a one-way analysis of variance (ANOVA) table followed by Tukey's HSD (honest significant difference) post hoc test. Crystal violet OD and CFUs were first natural log transformed due to their non-normal distribution as determined by a Q–Q plot. GraphPad Prism 8.2.0 (GraphPad Software) was used for calculations. A p-value of <0.05 was considered statistically significant. Statistically significant differences are reported on graphs as indicated with dissimilar letters. One standard deviation on the sample mean is reported. HGF experiments were performed twice (n = 5, 3 FOVs each); one representative experiment is shown. OK experiments were performed twice (n = 5, 2 FOVs

each) with the exception that OK activity following challenges (1 week, pH = 4.5 incubation) was performed once (n = 3, 3 FOVs each). *S. gordonii* experiments were performed at least twice (n = 3, multiple FOVs; LIVE/DEAD was performed at least six times with consistent results); one representative experiment is shown.

3. RESULTS AND DISCUSSION

Mono- and coimmobilization (at two ratios) of cell attaching peptide LamLG3 and antimicrobial peptide GL13K were achieved. Static WCAs (Figure 1A,B) demonstrated a hydrophilic surface following titanium etching (eTi; ca. 7.1° ± 2.7°) and silanization (eTi-sil; ca. 21.2° ± 3.9°) with a slight increase following LamLG3 monoimmobilization (21.5° ± 4.4°). However, LamLG3 showed a notable decrease in dynamic WCA through time (Figure 1C) unlike eTi and eTi-sil. The LamLG3 peptide could clearly reconfigure with the time of contact with water, which resulted in a dynamic wetting response of these coatings. GL13K monoimmobilization resulted in a highly hydrophobic surface (124.5° ± 11.3°), which in contrast to LamLG3 coatings showed a static wetting response. The static response of these coatings was likely related to the highly stable twisted nanoribbon structures formed by GL13K in solution, before being tethered on the surface, triggered by neutralization of cationic side groups of GL13K.[25,53]

Calculated surface fractional areas (Figure 1E) based on contact angles (96L/4G: ca. 26.3° ± 5.6° and 79L/21G: 44.9° ± 3.1°) demonstrated the ability to tune the surface fractional area for the resultant peptide coating simply based on pH. GL13K is more positively charged at pH = 9.04 than at pH = 9.42,[25] which can favor GL13K electrostatic attraction to the negatively charged surfaces. Therefore, more GL13K was recruited on the surface at pH = 9.04 vs pH = 9.42 (79L/21G and 96L/4G, respectively). Further, supporting the immobilization of the two peptides, WCAs demonstrated that surfaces with coimmobilized peptides (pictorially represented in Figure 1F) displayed the combined behavior of each of the two monopeptide samples, and images of the surfaces with fluorescently labeled peptides showed signals for each of the two peptides (Figure 1D). Moreover, surface fractional area calculations for 96L/4G through time (Figure S8) demonstrate, concomitant with the dynamic WCA, peptide rearrangement with time. XPS results (Figure 1G, Figure S5, and Table S1) also demonstrated the formation of the peptide coatings. N 1s and C 1s peaks are signature XPS signals for the peptides. N/Ti and C/Ti atom % ratios were greater than 0.5 and 2.5, respectively, for all peptide-laden groups and notably higher than controls, eTi and eTi-sil. Taken together, these results demonstrated that we successfully synthesized coatings with tunable surface fractional areas of coimmobilized peptides GL13K and LamLG3.

As a first tier of protection for infection-prone, high-failure-rate percutaneous osseointegrated devices, we cultured OKs on our coatings with the hypothesis that LamLG3 would increase proliferation, metabolic activity, cells spreading, and HD formation. After both 1 and 3 days of culture, OKs showed a statistically significant increase in metabolic activity (Figure 2A), proliferation (Figure 2B; Figure 2D shows DAPI-stained cells at day 3), and surface area (Figure 2C) for all LamLG3 contained groups (LamLG3, 96L/4G, and 79L/21G) compared to noncoated controls (eTi and eTi-sil) as well as monoimmobilized

GL13K. Interestingly, in many cases, no statistically significance differences were found between 96L/4G, 79L/21G, and monoimmobilized LamLG3 suggesting that a lower surface fractional area of LamLG3 on the surface was sufficient to induce positive OK activity. Furthermore, as we have previously reported, GL13K showed no detrimental effects (compared to controls eTi and eTi-sil) on the eukaryotic OKs.[30,38]

Motivated by these encouraging results that LamLG3 could stimulate OK proliferation at all surface fractional areas, we performed semiquantitative immunofluorescence against Collagen XVII, a late marker of HD formation, on all groups and controls.[50] Total fluorescent signal collected (Figure 3A; relative to eTi) showed a statistically significant increase in HD formation in all LamLG3-containing groups compared to controls (eTi and eTi-sil). Indeed, when normalized to the total number of cells in each FOV, this was again statistically significant (Figure 3B; representative micrographs at day 3 in Figure 3C). These results are consistent with past work that showed LamLG3 could stimulate OK proliferation and HD formation,[38] even *in vivo*.[54] Furthermore, we correlated the increase in HD formation in OKs to an increase in mechanical attachment using a centrifugation test (Figure S10); mechanically weak soft tissue attachment is a noted clinical deficiency.[18] Such a keratinocyte response may be able to promote rarely seen apical HD formation on dental implants. While inspiring previous work has engineered simultaneously antimicrobial and bone regenerating surfaces,[55–65] no work to date has focused on antimicrobial surfaces for implants with simultaneous soft tissue integration such as Figure 3 demonstrates.

As a second—and immediate—tier of protection for percutaneous osseointegrated devices, we evaluated the antimicrobial activity of our coatings against *S. gordonii,* a primary colonizer of dental implant surfaces. *S. gordonii* is critical to biofilm establishment and attachment of species such as *P. Porphyromonas gingivalis* and *Fusobacterium* spp. for later development and maturation.[66] As expected,[32] when we evaluated the antibiofilm activity by CFU/mL (Figure 4A), ATP bioluminescence (Figure 4B), and crystal violet biomass (Figure 4C), all groups containing GL13K, at any surface ratio, were significantly antimicrobial compared to eTi and eTi-sil controls without any detrimental effect from inclusion of LamLG3 in the coimmobilized groups at both surface fractional areas. Interestingly, based on monoimmobilized coatings of LamLG3, we unexpectedly observed that fewer *S. gordonii* colonized LamLG3 coated surfaces (Figure 4D) in comparison to GL13K monoimmobilized that formed thick, albeit dead, biofilms. This behavior was retained in the coimmobilized groups (96L/4G and 79L/21G; Figure 4E) such that *S. gordonii* biofilm is relatively sparse (i.e., LamLG3 activity) and there are localized areas of red (indicated by inset pointers in Figure 4E), an indication of dead bacteria (i.e., GL13K activity). Moreover, CFU/mL results (Figure 4A) indicate that LamLG3 does not seem to affect the ability of *S. gordonii* recovered from LamLG3 to grow, but rather functions as an antimicrobial surface by preventing fouling with *S. gordonii*, based on decreased biomass seen in Figure 4C and D micrographs. Antifouling and antibiofouling peptides have been developed[67]—typically fluorinated or self-assembling—but LamLG3 is not fluorinated and, although not yet studied, seemingly does not self-assemble. This anticolonization activity of LamLG3 is worth further investigation as it may be particularly relevant given recent attention to antimicrobials, including AMPs, indiscriminately killing both target species and “good” commensal bacteria species, thereby causing net harm to the multispecies microbial

community.[68,69] What is notable in our system is the stark difference in eukaryotic (pro-keratinocyte attachment and proliferation) and prokaryotic (anti-*S. gordonii*) responses. On the whole, our evidence (Figure 4) suggests that surfaces with coimmobilized peptides displayed a dual protection system against infection: anti-*S. gordonii* colonization from LamLG3 and bactericidal activity from GL13K. However, further *in vivo* verification of antimicrobial activity is necessary.

We were next curious to understand if LamLG3 was specific to keratinocytes or perhaps a more general cellular cue, such as the commonly used RGD (arginine-glycine-aspartate peptide) for dental implants.[70] Implant placement can be highly disruptive to surrounding tissue and result in colonization of implant surfaces with many cells types, such as HGFs.[21] However, the desired tissue regeneration—JE—is exclusively OKs, as only OKs are able to form HDs. The lack of exclusive OK colonization on dental implant surfaces contributes to parafunctional peri-implant JE regeneration. Interestingly, HGF metabolic activity (Figure 5A) and proliferation (Figure 5B; Figure 5C shows DAPI-stained cells at day 2) showed no response to LamLG3. A slight, but significant, decrease in HGF metabolic activity and proliferation for monoimmobilized GL13K was seen. However, we have previously shown that GL13K does not interfere with early osseointegration in a rabbit model compared to noncoated controls.[35] Responses, or lack thereof, to LamLG3 are likely integrin mediated, as HGFs and OKs have different integrin expression profiles.[71,72] An exact, mechanistic understanding of our observed cell selectivity phenomena is one branch of our current work which may enable further peptide-mediated control of keratinocytes.[73] While past work has successfully engineered cell-specific surfaces,[74,75] to the best of our knowledge this is first report of a cell-specific, multifunctional peptide coating.

We were further interested in the stability of our coatings under simulated clinical conditions. An oft-cited drawback for the use of biomolecules for surface coatings is their perceived instability.[76] We have previously shown the marked stability of monoimmobilized GL13K coatings but had posited that this was due to the remarkably hydrophobic character of such surfaces, which would likely not apply to the stability of hydrophilic LamLG3 coatings.[40] We ultrasonicated and then measured WCAs for our coatings after 1 and 2 h at both a biofilm-relevant pH = 4.5 and a control pH = 7.4 (Figure 6A). Coatings demonstrated relatively small changes in WCA compared to virgin samples. The statistically significantly larger changes in WCA (Figure 6A) in eTi-sil compared to other groups may be related to the susceptibility for hydrolysis of the unprotected siloxanes in the silane layer. XPS analysis of the challenged surfaces also showed that the peptide coatings were retained after 1 week incubation at both pHs (Figure S6 and Table S2, pH = 4.5; and Figure S7 and Table S3, pH = 7.4). Fluorescently tagged peptides were even retained after incubation in fresh saliva for 14 days (Figure S9). Overall, these results demonstrated that our coatings were robust against simulated oral challenges, as previously proven for other antimicrobial peptide coated surfaces.[77,78] However, we note that since we used purified saliva, some enzymes that may degrade peptides may be lost. Siloxane layer hydrolysis may also contribute to peptide loss. Most importantly, OKs significantly responded (metabolic activity, Figure 6B; proliferation, Figure 6C; and HD formation, Figure 6D) to LamLG3 1-week challenged similarly to virgin, newly synthesized samples (Figure 2 and Figure 3). OK hemidesmosome formation, a process mediated by integrins and laminin 332, is illustrated

in Figure 6E. Collagen XVII is critical to this process and contains multiple binding sites for relevant proteins such as plectin, BPAG1e, integrin β4, integrin α6, and laminin 332.[79]

4. CONCLUSIONS

We successfully engineered tunable, multifunctional implant surfaces with coimmobilized peptides simultaneously capable of (a) enhancing keratinocyte proliferation and hemidesmosome formation, (b) unaltered fibroblast proliferation, and (c) demonstrating antibiofilm activity against *Streptococcus gordonii*. Our coating showed stability and retained activity against mechanical and thermochemical challenges, suggesting their intraoral durability. These multifunctional surfaces may be used on dental and other percutaneous implants to reduce infection and failure rates.

Supplementary Material

Refer to Web version on PubMed Central for supplementary material.

ACKNOWLEDGMENTS

The authors thank Ruoqiong Chen, Cole Homer, and Michael Weston for technical assistance for microbiology experiments, centrifugation experiments, and disk fabrication, respectively. Figures were partially created with BioRender. Parts of this work were carried out in the University of Minnesota I.T. Characterization Facility, which receives partial support from NSF through the MRSEC program. NGF acknowledges support from a 3M Science and Technology Fellowship. Research reported in this publication was supported by the National Institute of Dental & Craniofacial Research of the National Institutes of Health under Award Number R01DE026117 to C.A., T90DE0227232 to N.G.F., and R90DE023058 to D.G.M. The content is solely the responsibility of the authors and does not necessarily represent the official views of the National Institutes of Health.

REFERENCES

(1). O'Niel MB; Runge CL; Friedland DR; Kerschner JE Patient Outcomes in Magnet-Based Implantable Auditory Assist Devices. JAMA Otolaryngol. - Head Neck Surg 2014, 140 (6), 513–520. [PubMed: 24763485]

(2). Hernandez GA; Nunez Breton JD; Chaparro SV Driveline Infection in Ventricular Assist Devices and Its Implication in the Present Era of Destination Therapy. Open J. Cardiovasc. Surg 2017, 9, 117906521771421.

(3). Overmann AL; Aparicio C; Richards JT; Mutreja I; Fischer NG; Wade SM; Potter BK; Davis TA; Bechtold JE; Forsberg JA; Dey D Orthopaedic Osseointegration: Implantology and Future Directions. J. Orthop. Res 2020, 38 (7), 1445–1454. [PubMed: 31876306]

(4). Jacobsen SM; Stickler DJ; Mobley HLT; Shirtliff ME Complicated Catheter-Associated Urinary Tract Infections Due to Escherichia Coli and Proteus Mirabilis. Clin. Microbiol. Rev 2008, 21 (1), 26–59. [PubMed: 18202436]

(5). Elani HW; Starr JR; Da Silva JD; Gallucci GO Trends in Dental Implant Use in the U.S., 1999–2016, and Projections to 2026. J. Dent. Res 2018, 97 (13), 1424–1430. [PubMed: 30075090]

(6). Dental Implants: Market Estimates and Trends Analysis; Grand View Research, 2017.

(7). Tarnow DP Increasing Prevalence of Peri-Implantitis. J. Dent. Res 2016, 95 (1), 7–8. [PubMed: 26701918]

(8). Figuero E; Graziani F; Sanz I; Herrera D; Sanz M Management of Peri-Implant Mucositis and Peri-Implantitis. Periodontol. 2000 2014, 66 (1), 255–273. [PubMed: 25123773]

(9). Chrcanovic BR; Kisch J; Albrektsson T; Wennerberg A A Retrospective Study on Clinical and Radiological Outcomes of Oral Implants in Patients Followed up for a Minimum of 20 Years. Clin. Implant Dent. Relat. Res 2018, 20 (2), 199–207. [PubMed: 29210186]

(10). Heitz-Mayfield LJA Peri-Implant Diseases: Diagnosis and Risk Indicators. J. Clin. Periodontol 2008, 35, 292–304. [PubMed: 18724857]

(11). Cochran D; Froum S Academy Report: Peri-Implant Mucositis and Peri-Implantitis: A Current Understanding of Their Diagnoses and Clinical Implications. J. Periodontol 2013, 84 (4), 436–443. [PubMed: 23537178]

(12). Lamont RJ; Koo H; Hajishengallis G The Oral Microbiota: Dynamic Communities and Host Interactions. Nat. Rev. Microbiol 2018, 16 (12), 745–759. [PubMed: 30301974]

(13). Lee CT; Huang YW; Zhu L; Weltman R Prevalences of Peri-Implantitis and Peri-Implant Mucositis: Systematic Review and Meta-Analysis. J. Dent 2017, 62, 1–12. [PubMed: 28478213]

(14). Fischer NG; Münchow EA; Tamerler C; Bottino MC; Aparicio C Harnessing Biomolecules for Bioinspired Dental Biomaterials. J. Mater. Chem. B 2020, DOI: 10.1039/D0TB01456G.

(15). Hormia M; Sahlberg C; Thesleff I; Airenne T The Epithelium-Tooth Interface–a Basal Lamina Rich in Laminin-5 and Lacking Other Known Laminin Isoforms. J. Dent. Res 1998, 77 (7), 1479–1485. [PubMed: 9663432]

(16). Marinkovich MP Tumour Microenvironment: Laminin 332 in Squamous-Cell Carcinoma. Nat. Rev. Cancer 2007, 7 (5), 370–380. [PubMed: 17457303]

(17). Walko G; Castañón MJ; Wiche G Molecular Architecture and Function of the Hemidesmosome. Cell Tissue Res 2015, 360 (2), 363–378. [PubMed: 25487405]

(18). Atsuta I; Ayukawa Y; Kondo R; Oshiro W; Matsuura Y; Furuhashi A; Tsukiyama Y; Koyano K Soft Tissue Sealing around Dental Implants Based on Histological Interpretation. J. Prosthodont. Res 2016, 60 (1), 3–11. [PubMed: 26725967]

(19). Wazen RM; Moffatt P; Ponce KJ; Kuroda S; Nishio C; Nanci A Inactivation of the Odontogenic Ameloblast-Associated Gene Affects the Integrity of the Junctional Epithelium and Gingival Healing. Eur. Cells Mater 2015, 30, 187–199.

(20). Wright JT Oral Manifestations in the Epidermolysis Bullosa Spectrum. Dermatol. Clin 2010, 28 (1), 159–164. [PubMed: 19945630]

(21). Esposito M; Maghaireh H; Grusovin MG; Ziounas I; Worthington HV Soft Tissue Management for Dental Implants: What Are the Most Effective Techniques? A Cochrane Systematic Review. Eur. J. Oral Implantol 2012, 5 (3), 221–238. [PubMed: 23000707]

(22). Bosshardt DD Soft Tissue Wound Healing around Teeth and Dental Implants. 2014, 41, 6–22 DOI: DOI: 10.1111/jcpe.12206.

(23). Laird NZ; Malkawi WI; Chakka JL; Acri T; Elangovan S; Salem AK A Proof of Concept Gene-Activated Titanium Surface for Oral Implantology Applications. J. Tissue Eng. Regener. Med 2020, 14, 622.

(24). Peschel A; Sahl H-G The Co-Evolution of Host Cationic Antimicrobial Peptides and Microbial Resistance. Nat. Rev. Microbiol 2006, 4 (7), 529–536. [PubMed: 16778838]

(25). Ye Z; Zhu X; Acosta S; Kumar D; Sang T; Aparicio C Self-assembly dynamics and antimicrobial activity of all l - and d-amino acid enantiomers of a designer peptide. Nanoscale 2019, 11 (1), 266–275.

(26). Ye Z; Aparicio C Modulation of Supramolecular Self-Assembly of an Antimicrobial Designer Peptide by Single Amino Acid Substitution: Implications on Peptide Activity. Nanoscale Adv 2019, 1 (12), 4679–4682. [PubMed: 31844837]

(27). Gorr S-U; Abdolhosseini M; Shelar A; Sotsky J Dual Host-Defence Functions of SPLUNC2/PSP and Synthetic Peptides Derived from the Protein. Biochem. Soc. Trans 2011, 39 (4), 1028–1032. [PubMed: 21787342]

(28). Hirt H; Gorr SU Antimicrobial Peptide GL13K Is Effective in Reducing Biofilms of Pseudomonas Aeruginosa. Antimicrob. Agents Chemother 2013, 57 (10), 4903–4910. [PubMed: 23917321]

(29). Chen X Multi-Bioactive Peptide Coatings for Dental Implants; PhD Dissertation; University of Minnesota School of Dentistry, 2014.

(30). Holmberg KV; Abdolhosseini M; Li Y; Chen X; Gorr SU; Aparicio C Bio-Inspired Stable Antimicrobial Peptide Coatings for Dental Applications. Acta Biomater. 2013, 9 (9), 8224–8231. [PubMed: 23791670]

(31). Acosta S; Quintanilla L; Alonso M; Aparicio C; Rodríguez-Cabello JC Recombinant AMP/Polypeptide Self-Assembled Monolayers with Synergistic Antimicrobial Properties for Bacterial Strains of Medical Relevance. ACS Biomater. Sci. Eng 2019, 5 (9), 4708–4716.

(32). Moussa DG; Fok A; Aparicio C Hydrophobic and Antimicrobial Dentin: A Peptide-Based 2-Tier Protective System for Dental Resin Composite Restorations. Acta Biomater 2019, 88, 251–265. [PubMed: 30753942]

(33). Gorr SU; Flory CM; Schumacher RJ In Vivo Activity and Low Toxicity of the Second-Generation Antimicrobial Peptide DGL13K. PLoS One 2019, 14 (5), 1–14.

(34). Hirt H; Hall JW; Larson E; Gorr S A D-Enantiomer of the Antimicrobial Peptide GL13K Evades Antimicrobial Resistance in the Gram Positive Bacteria Enterococcus Faecalis and Streptococcus Gordonii. 2018, 1–16. DOI: 10.1371/journal.pone.0194900.

(35). Chen X; Zhou XC; Liu S; Wu RF; Aparicio C; Wu JY In Vivo Osseointegration of Dental Implants with an Antimicrobial Peptide Coating. J. Mater. Sci.: Mater. Med 2017, 28 (5), 76. [PubMed: 28386851]

(36). Kim JM; Park WH; Min BM The PPFLMLLKGSTR Motif in Globular Domain 3 of the Human Laminin-5 A3 Chain Is Crucial for Integrin A3β1 Binding and Cell Adhesion. Exp. Cell Res 2005, 304 (1), 317–327. [PubMed: 15707596]

(37). Werner S; Huck O; Frisch B; Vautier D; Elkaim R; Voegel JC; Brunel G; Tenenbaum H The Effect of Micro-structured Surfaces and Laminin-Derived Peptide Coatings on Soft Tissue Interactions with Titanium Dental Implants. Biomaterials 2009, 30 (12), 2291–2301. [PubMed: 19168216]

(38). Koidou VP; Argyris PP; Skoe EP; Mota Siqueira J; Chen X; Zhang L; Hinrichs JE; Costalonga M; Aparicio C Peptide Coatings Enhance Keratinocyte Attachment towards Improving the Peri-Implant Mucosal Seal. Biomater. Sci 2018, 6 (7), 1936–1945. [PubMed: 29850754]

(39). Fischer NG; He J; Aparicio C Surface Immobilization Chemistry of a Laminin-Derived Peptide Affects Keratinocyte Activity. Coatings 2020, 10 (6), 560. [PubMed: 32855816]

(40). Chen X; Hirt H; Li Y; Gorr S-U; Aparicio C Antimicrobial GL13K Peptide Coatings Killed and Ruptured the Wall of Streptococcus Gordonii and Prevented Formation and Growth of Biofilms. PLoS One 2014, 9 (11), No. e111579. [PubMed: 25372402]

(41). Chen X; Sevilla P; Aparicio C Surface Biofunctionalization by Covalent Co-Immobilization of Oligopeptides. Colloids Surf., B 2013, 107, 189–197.

(42). Sevilla P; Gil J; Aparicio C Relevant Properties for Immobilizing Short Peptides on Biosurfaces. IRBM 2017, 38 (5), 256–265.

(43). Diao L; Meibohm B Pharmacokinetics and Pharmacokinetic-Pharmacodynamic Correlations of Therapeutic Peptides. Clin. Pharmacokinet 2013, 52 (10), 855–868. [PubMed: 23719681]

(44). Cassie ABD; Baxter S Wettability of Porous Surfaces. Trans. Faraday Soc 1944, 40 (5), 546.

(45). Bormashenko E Physics of Solid–Liquid Interfaces: From the Young Equation to the Superhydrophobicity. Low Temp. Phys 2016, 42 (8), 622–635.

(46). Israelachvili JN; Gee ML Contact Angles on Chemically Heterogeneous Surfaces. Langmuir 1989, 5 (1), 288–289.

(47). Wang J; Bratko D; Luzar A Probing Surface Tension Additivity on Chemically Heterogeneous Surfaces by a Molecular Approach. Proc. Natl. Acad. Sci. U. S. A 2011, 108 (16), 6374–6379. [PubMed: 21460249]

(48). Khatayevich D; So CR; Hayamizu Y; Gresswell C; Sarikaya M Controlling the Surface Chemistry of Graphite by Engineered Self-Assembled Peptides. Langmuir 2012, 28 (23), 8589–8593. [PubMed: 22428620]

(49). Dickson MA; Hahn WC; Ino Y; Ronfard V; Wu JY; Weinberg RA; Louis DN; Li FP; Rheinwald JG Human Keratinocytes That Express HTERT and Also Bypass a P16INK4a-Enforced Mechanism That Limits Life Span Become Immortal yet Retain Normal Growth and Differentiation Characteristics. Mol. Cell. Biol 2000, 20 (4), 1436–1447. [PubMed: 10648628]

(50). Van den Bergh F; Eliason SL; Giudice GJ Type XVII Collagen (BP180) Can Function as a Cell–matrix Adhesion Molecule via Binding to Laminin 332. Matrix Biol. 2011, 30 (2), 100–108. [PubMed: 21034821]

(51). Guillem-Marti J; Gelabert M; Heras-Parets A; Pegueroles M; Ginebra MP; Manero JM RGD Mutation of the Heparin Binding II Fragment of Fibronectin for Guiding Mesenchymal Stem Cell Behavior on Titanium Surfaces. ACS Appl. Mater. Interfaces 2019, 11 (4), 3666–3678. [PubMed: 30607934]

(52). Reyes CD; García AJ A Centrifugation Cell Adhesion Assay for High-Throughput Screening of Biomaterial Surfaces. J. Biomed. Mater. Res., Part A 2003, 67 (1), 328–333.

(53). Moussa DG; Kirihara JA; Ye Z; Fischer NG; Khot J; Witthuhn BA; Aparicio C Dentin Priming with Amphipathic Antimicrobial Peptides. J. Dent. Res 2019, 98 (10), 1112–1121. [PubMed: 31313946]

(54). Liu Z; Ma S; Lu X; Zhang T; Sun Y; Feng W; Zheng G; Sui L; Wu X; Zhang X; Gao P Reinforcement of Epithelial Sealing around Titanium Dental Implants by Chimeric Peptides. Chem. Eng. J 2019, 356, 117–129.

(55). Raphel J; Holodniy M; Goodman SB; Heilshorn SC Multifunctional Coatings to Simultaneously Promote Osseointegration and Prevent Infection of Orthopaedic Implants. Biomaterials 2016, 84, 301–314. [PubMed: 26851394]

(56). Hoyos-Nogués M; Velasco F; Ginebra MP; Manero JM; Gil FJ; Mas-Moruno C Regenerating Bone via Multifunctional Coatings: The Blending of Cell Integration and Bacterial Inhibition Properties on the Surface of Biomaterials. ACS Appl. Mater. Interfaces 2017, 9 (26), 21618–21630. [PubMed: 28594999]

(57). Choi B-H; Jo YK; Zhou C; Jang H-S; Ahn J-S; Jun SH; Cha HJ Sticky Bone-Specific Artificial Extracellular Matrix for Stem Cell-Mediated Rapid Craniofacial Bone Therapy. Appl. Mater. Today 2020, 18, 100531.

(58). Lin W; Junjian C; Chengzhi C; Lin S; Sa L; Li R; Yingjun W Multi-Biofunctionalization of a Titanium Surface with a Mixture of Peptides to Achieve Excellent Antimicrobial Activity and Biocompatibility. J. Mater. Chem. B 2015, 3 (1), 30–33. [PubMed: 32261920]

(59). Kumeria T; Mon H; Aw MS; Gulati K; Santos A; Griesser HJ; Losic D Advanced Biopolymer-Coated Drug-Releasing Titania Nanotubes (TNTs) Implants with Simultaneously Enhanced Osteoblast Adhesion and Antibacterial Properties. Colloids Surf., B 2015, 130, 255–263.

(60). Subbiahdoss G; Pidhatika B; Coullerez G; Charnley M; Kuijer R; van der Mei H; Textor M; Busscher H Bacterial Biofilm Formation versus Mammalian Cell Growth on Titanium-Based Mono- and Bi-Functional Coating. Eur. Cells Mater 2010, 19, 205–213.

(61). Jiao Y; Tay FR; Niu L; Chen J Advancing Antimicrobial Strategies for Managing Oral Biofilm Infections. Int. J. Oral Sci 2019, 11 (3), 28. [PubMed: 31570700]

(62). Mas-Moruno C; Su B; Dalby MJ Multifunctional Coatings and Nanotopographies: Toward Cell Instructive and Antibacterial Implants. Adv. Healthcare Mater 2019, 8 (1), 1801103.

(63). Yuran S; Dolid A; Reches M Resisting Bacteria and Attracting Cells: Spontaneous Formation of a Bifunctional Peptide-Based Coating by On-Surface Assembly Approach. ACS Biomater. Sci. Eng 2018, 4 (12), 4051–4061.

(64). Yeo I-S; Min S-K; Kang HK; Kwon T-K; Jung SY; Min B-M Identification of a Bioactive Core Sequence from Human Laminin and Its Applicability to Tissue Engineering. Biomaterials 2015, 73, 96–109. [PubMed: 26406450]

(65). Wu H; Liu T; Xu Z; Qian J; Shen X; Li Y; Pan Y; Wang D; Zheng K; Boccaccini AR; Wei J Enhanced Bacteriostatic Activity, Osteogenesis and Osseointegration of Silicon Nitride/Polyetherketoneketone Composites with Femtosecond Laser Induced Micro/Nano Structural Surface. Appl. Mater. Today 2020, 18, 1–15.

(66). Kinane DF; Stathopoulou PG; Papapanou PN Periodontal Diseases. Nat. Rev. Dis. Prim 2017, 3, 17038. [PubMed: 28805207]

(67). Sakala GP; Reches M Peptide-Based Approaches to Fight Biofouling. Adv. Mater. Interfaces 2018, 5 (18), 1800073.

(68). Bhalodi AA; van Engelen TSR; Virk HS; Wiersinga WJ Impact of Antimicrobial Therapy on the Gut Microbiome. J. Antimicrob. Chemother 2019, 74, i6–i15. [PubMed: 30690540]

(69). Mondhe M; Chessher A; Goh S; Good L; Stach JEM Species-Selective Killing of Bacteria by Antimicrobial Peptide-PNAs. PLoS One 2014, 9 (2), e89082. [PubMed: 24558473]

(70). Schliephake H; Scharnweber D; Dard M; Rössler S; Sewing A; Meyer J; Hoogestraat D Effect of RGD Peptide Coating of Titanium Implants on Periimplant Bone Formation in the Alveolar Crest. An Experimental Pilot Study in Dogs. Clin. Oral Implants Res 2002, 13 (3), 312–319. [PubMed: 12010163]

(71). Guo F; Carter DE; Mukhopadhyay A; Leask A Gingival Fibroblasts Display Reduced Adhesion and Spreading on Extracellular Matrix: A Possible Basis for Scarless Tissue Repair? PLoS One 2011, 6 (11), e27097. [PubMed: 22073262]

(72). Oates CJ; Wen W; Hamilton DW Role of Titanium Surface Topography and Surface Wettability on Focal Adhesion Kinase Mediated Signaling in Fibroblasts. Materials 2011, 4 (12), 893–907. [PubMed: 28879956]

(73). Davis-Hall D; Nguyen V; D'Ovidio TJ; Tsai E; Bilousova G; Magin CM Peptide-Functionalized Hydrogels Modulate Integrin Expression and Stemness in Adult Human Epidermal Keratinocytes. Adv. Biosyst 2019, 3 (10), 1900022.

(74). Kam L; Shain W; Turner JN; Bizios R Selective Adhesion of Astrocytes to Surfaces Modified with Immobilized Peptides. Biomaterials 2002, 23 (2), 511–515. [PubMed: 11761172]

(75). Yu S; Zuo X; Shen T; Duan Y; Mao Z; Gao C A Density Gradient of VAPG Peptides on a Cell-Resisting Surface Achieves Selective Adhesion and Directional Migration of Smooth Muscle Cells over Fibroblasts. Acta Biomater. 2018, 72, 70–81. [PubMed: 29635070]

(76). Collier JH; Segura T Evolving the Use of Peptides as Components of Biomaterials. Biomaterials 2011, 32 (18), 4198–4204. [PubMed: 21515167]

(77). Wisdom EC; Zhou Y; Chen C; Tamerler C; Snead ML Mitigation of Peri-Implantitis by Rational Design of Bifunctional Peptides with Antimicrobial Properties. ACS Biomater. Sci. Eng 2020, 6 (5), 2682–2695. [PubMed: 32467858]

(78). Wisdom C; Chen C; Yuca E; Zhou Y; Tamerler C; Snead ML Repeatedly Applied Peptide Film Kills Bacteria on Dental Implants. JOM 2019, 71 (4), 1271–1280. [PubMed: 31178649]

(79). Borradori L; Sonnenberg A Structure and Function of Hemidesmosomes: More than Simple Adhesion Complexes. J. Invest. Dermatol 1999, 112 (4), 411–418. [PubMed: 10201522]

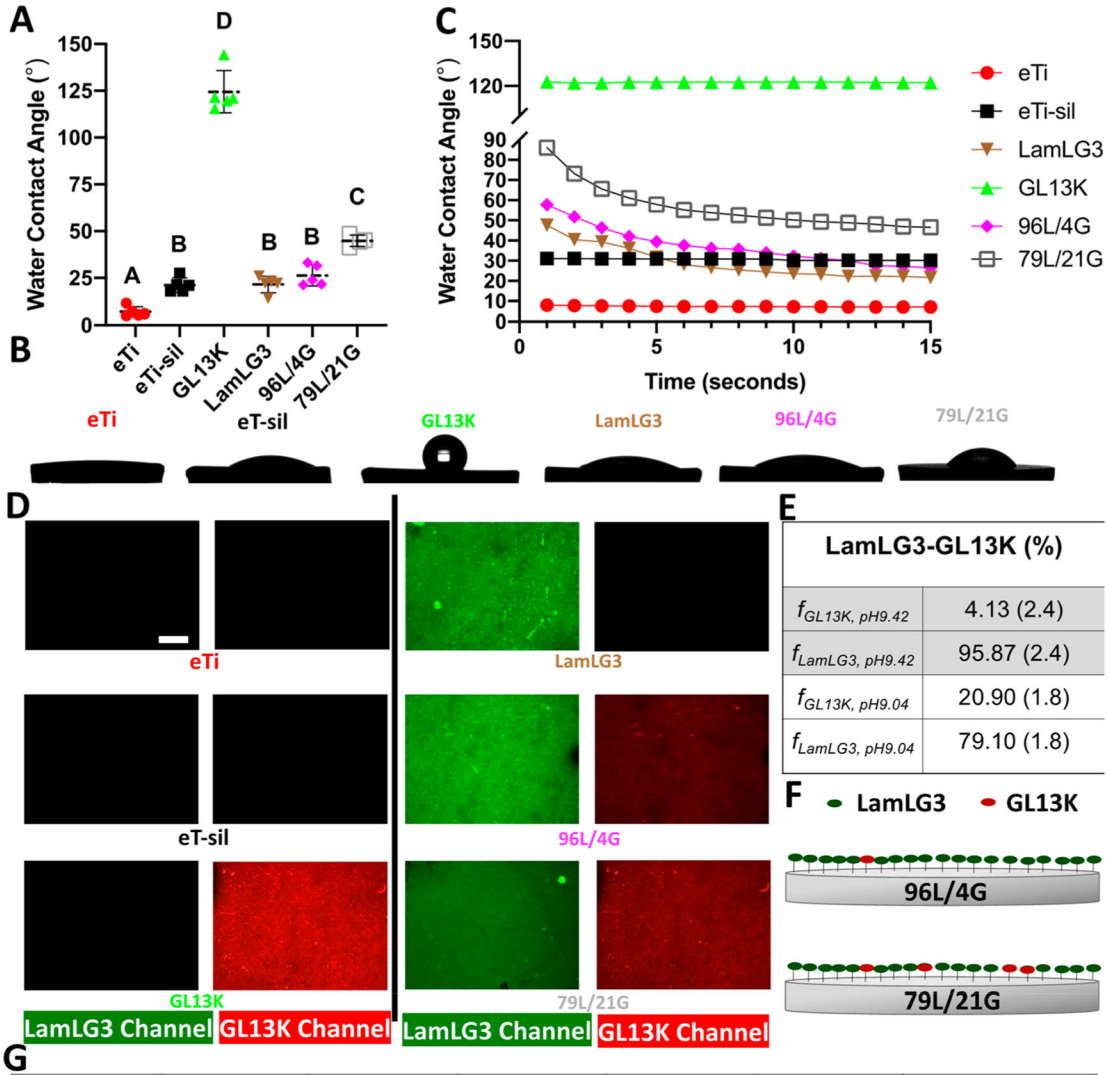

G

Coating ▶ ▼*At % Ratio*	eTi	eT-sil	GL13K	LamLG3	96L/4G	79L/21G
N/Ti	0	0.01	0.82	2.54	0.57	0.86
C/Ti	0.4	0.83	3.55	9.87	2.51	3.48

Figure 1.

Characterization of mono- and coimmobilized peptide coatings. (A) Water contact angle at equilibrium. (B) Photographs of water drops at equilibrium. (C) Dynamic water contact angle through 15 s (one representative experiment). (D) Visualization of fluorescently tagged peptides (LamLG3-green and GL13K-red). (E) Calculated mean peptide surface fractional area for surfaces with coimmobilized peptides at pH = 9.42 (96L/4G) or pH = 9.04 (79L/21G). Standard deviations are shown between brackets. (F) Schematic demonstrating two peptide surface fractional areas; 96L/4G (top) and 79L/21G (bottom). (G) XPS atomic % ratio (At % ratio), N/Ti and C/Ti, for surfaces before and after peptide immobilization. Scale bar is 100 μm. A p-value of <0.05 was considered statistically significant.

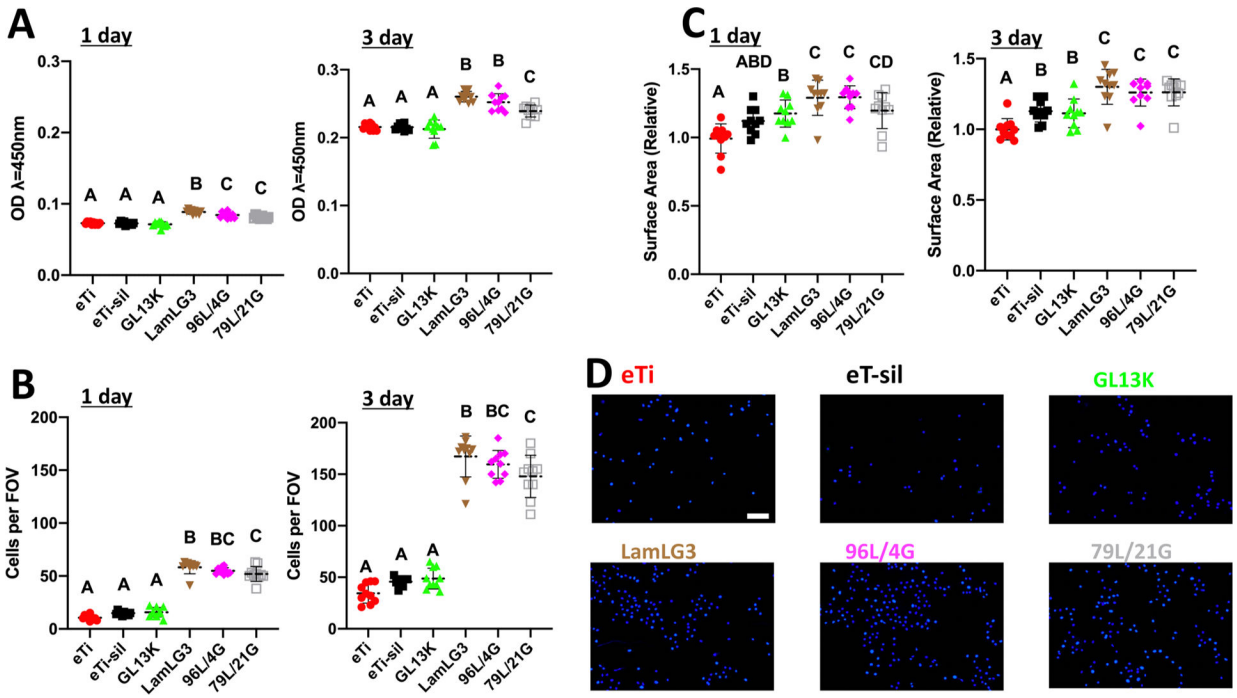

Figure 2.

Proliferation and cell spreading of oral keratinocytes on peptide coatings and controls. (A) Metabolic activity (CCK8) of keratinocytes at 1 day and 3 days. (B) Number of keratinocytes per field of view (FOV) at 1 day and 3 days. (C) Surface area occupied per keratinocyte relative to eTi control at 1 day and 3 days. (D) Immunofluorescent micrographs (DAPI-stained) of keratinocytes at 3 days. Scale bar is 100 μm. A p-value of <0.05 was considered statistically significant.

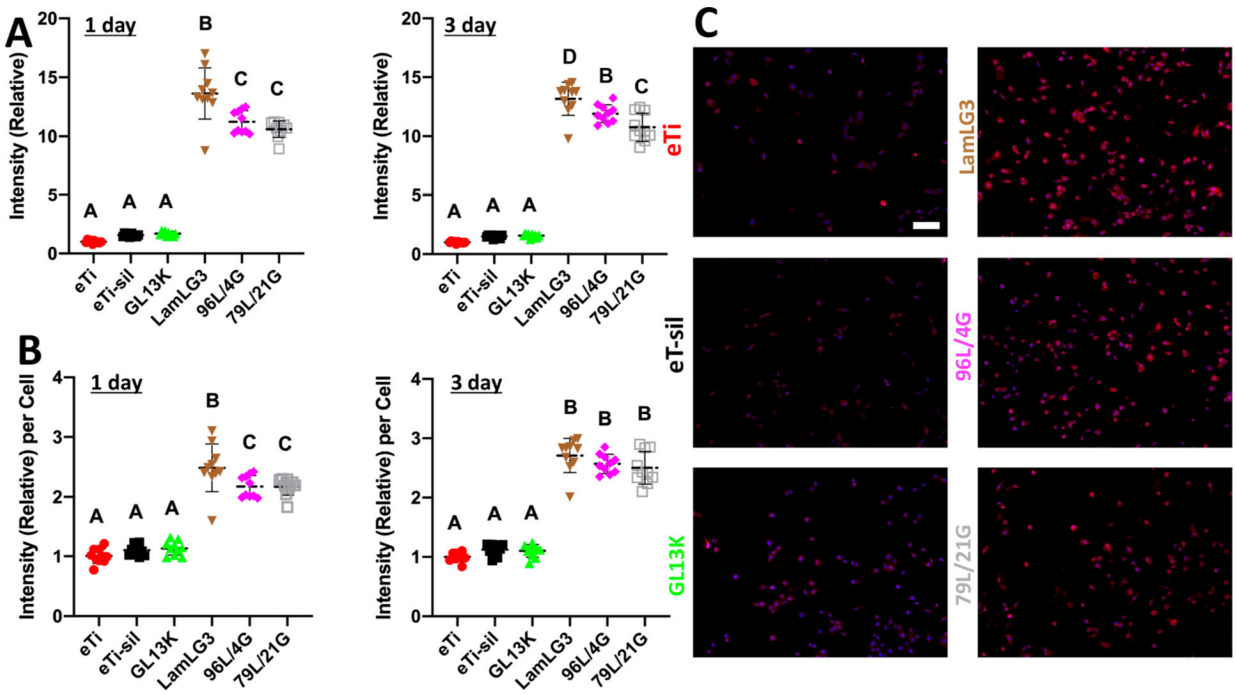

Figure 3.

Hemidesmosome formation (Collagen XVII) of oral keratinocytes on peptide coatings and controls. (A) Total immunofluorescent intensity (Collagen XVII) of keratinocytes relative to eTi control at 1 day and 3 days per field of view (FOV). (B) Immunofluorescent intensity (Collagen XVII) per keratinocyte relative to eTi control at 1 day and 3 days. (C) Immunofluorescent micrographs (DAPI-blue and Collagen XVII-red) of keratinocytes at 3 days. Scale bar is 100 μm. A p-value of <0.05 was considered statistically significant.

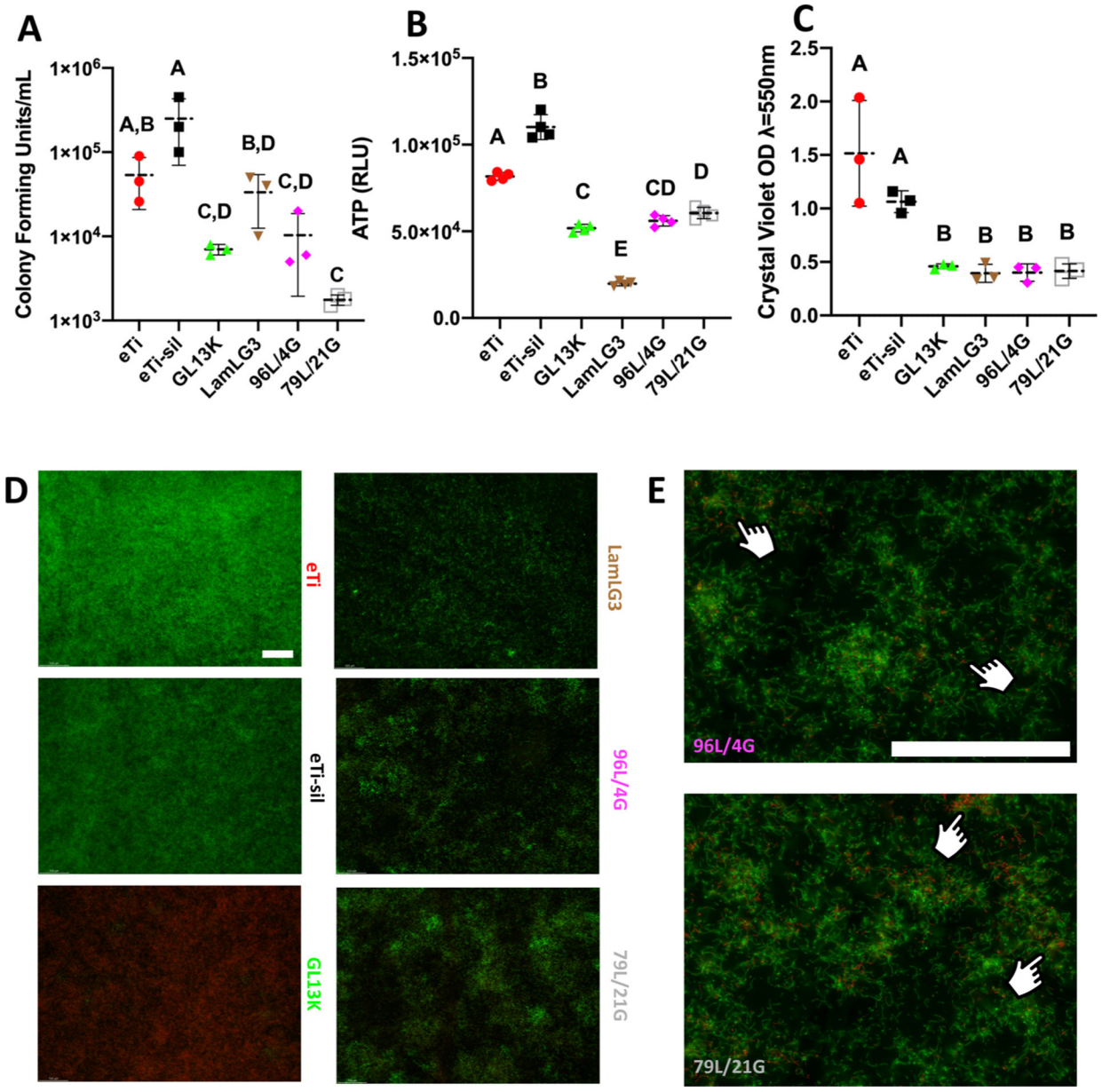

Figure 4.

Antimicrobial activity of peptide coatings and controls against *S. gordonii.* (A) Colony Forming Units (CFUs) per mL. (B) ATP bioluminescence and (C) Crystal violet biomass of *S. gordonii.* (D) LIVE/DEAD micrographs of *S. gordonii* at ×10. (E) LIVE/DEAD micrographs at ×40. Fingers denote localized area of red (nonvital) staining. Scale bar is 100 μm for both magnifications. A p-value of <0.05 was considered statistically significant.

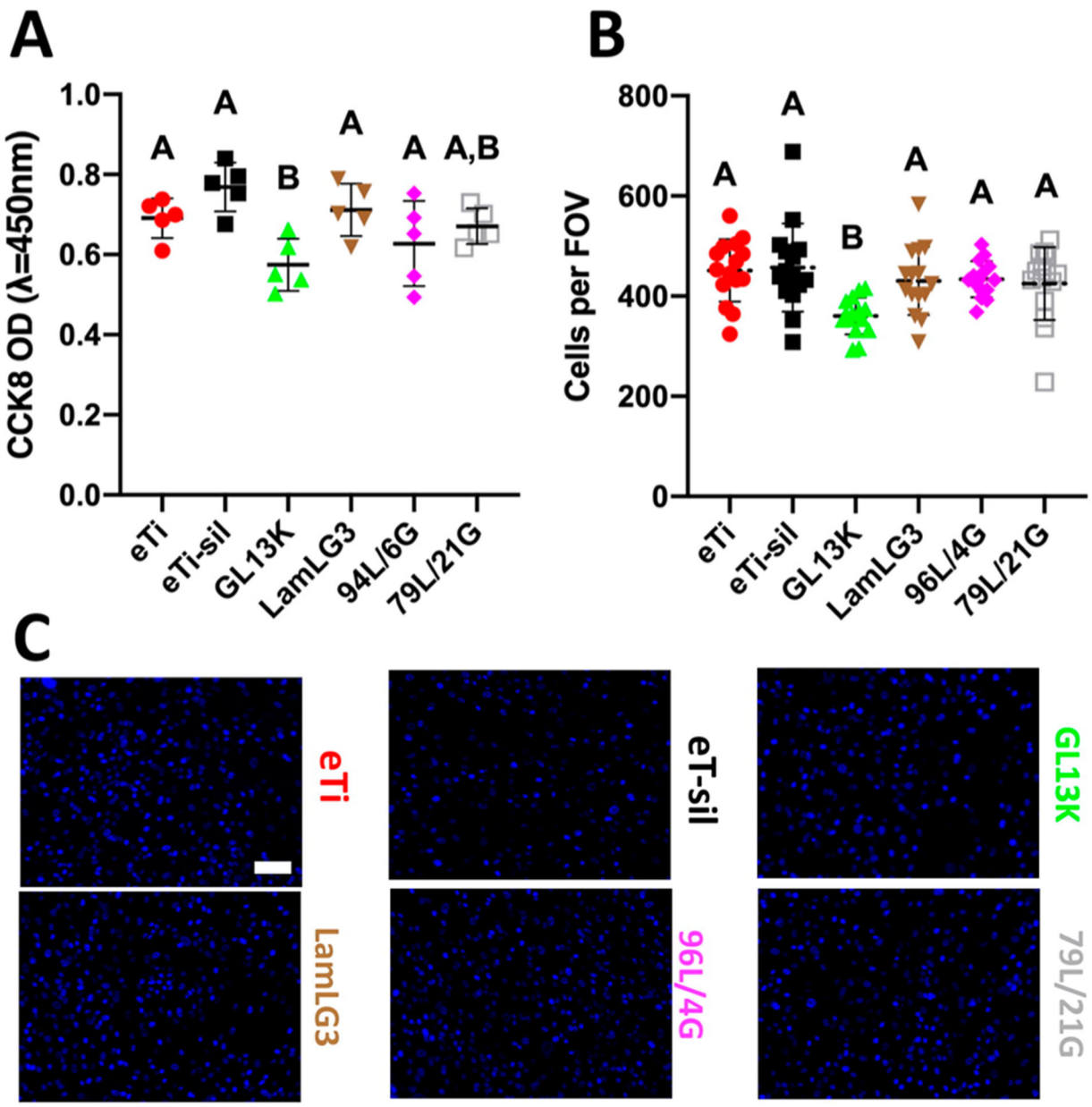

Figure 5.

Gingival fibroblast proliferation on coatings and controls. (A) Metabolic activity (CCK8) of fibroblasts at 2 days. (B) Number of fibroblasts per field of view (FOV) at 2 days. (C) Immunofluorescent micrographs (DAPI-stained) of fibroblasts at 2 days. Scale bar is 100 μm. A p-value of <0.05 was considered statistically significant.

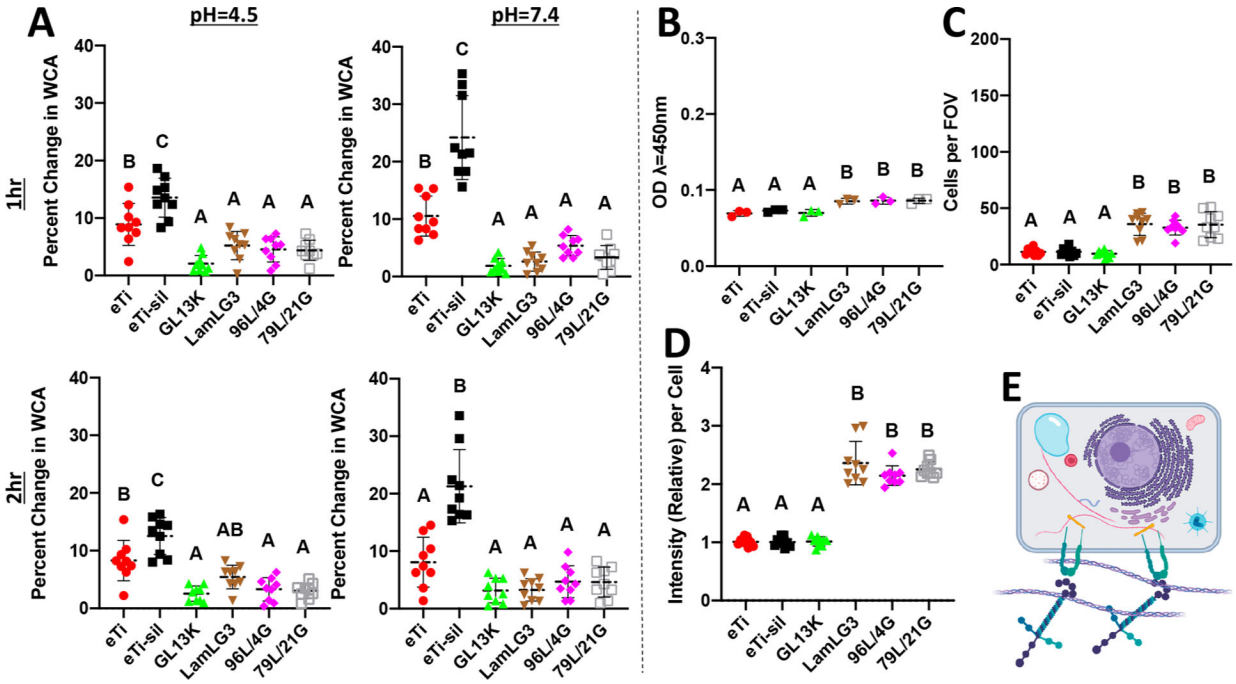

Figure 6.

Characterization of physical–chemical properties and biological activity of peptide coatings after oral-simulative challenges. (A) Water contact angle after 1 h sonication at pH = 4.5 (top left), pH = 7.4 (top right), 2 h sonication at pH = 4.5 (bottom left), and pH = 7.4 (bottom right). (B) Metabolic activity (CCK8) of keratinocytes at 1 day on pH = 4.5, 37 °C, 1 week challenged disks. (C) Number of keratinocytes per field of view (FOV) at 1 day on pH = 4.5, 37 °C, 1 week challenged disks. (D) Immunofluorescent intensity (Collagen XVII) per keratinocyte relative to eTi control at 1 day on pH = 4.5, 37 °C, 1 week challenged disks. (E) Schematic illustrating keratinocyte hemidesmosome formation.